https://doi.org/10.5194/essd-2020-250
Preprint. Discussion started: 28 October 2020

Two decades of distributed global radiation time series across a mountainous semiarid area (Sierra Nevada, Spain)

Cristina Aguilar[1], Rafael Pimentel[1], María J. Polo[1]

[1]Fluvial Dynamics and Hydrology Research Group, Andalusian Institute of Earth System Research, University of Cordoba, Cordoba, Spain

Correspondence to: Cristina Aguilar (caguilar@uco.es)

Abstract. The main drawback of the reconstruction of high resolution distributed global radiation (R_g) time series in mountainous semiarid environments is the common lack of station-based solar radiation registers. This work presents nineteen years (2000-2018) of high spatial resolution (30m x 30m) monthly and annual global radiation maps derived using the model proposed by Aguilar et al. (2010), driven by in situ daily global radiation measurements, from sixteen weather stations with historical records in the area, and a high resolution digital elevation model in a mountainous area in southern Europe: Sierra Nevada (SN) Mountain Range (Spain). The applicability of the modeling scheme was validated against daily global radiation registers at the weather stations with mean RMSE values of 2.63 MJ m^{-2} day^{-1} and best estimations on clear-sky days. Filled daily R_g at weather stations revealed quite stable minimum daily R_g values and greater variations in the maximum daily R_g, but no clear trends with altitude in any of the statistics unlike the analysis at the monthly and annual scale when there is an increase in the high extreme statistics with the altitude of the weather station, especially above 1500 m a.s.l. Monthly distributed R_g time series showed significant spatial differences of up to 200 MJ m^{-2} $month^{-1}$ that clearly followed the terrain configuration. July and December were clearly the months with the highest and lowest values of R_g received and the highest dispersion in the monthly R_g values was found in the spring and fall months. The great heterogeneity found in the monthly distribution of R_g along the study period (2000-2018), especially at the wet season, finally determined the inter annual differences of up to 800 MJ m^{-2} $year^{-1}$ in the incoming global radiation in SN. The time series of the surface global radiation datasets here provided can be used to analyze trends, inter-annual and seasonal variation characteristics of the global radiation received in SN with high spatial detail (30 m). Datasets are available at https://doi.pangaea.de/10.1594/PANGAEA.921012 (Aguilar et al., 2020).

1 Introduction

High mountain areas in semiarid environments present singular characteristics due to the continuous interaction of alpine conditions in the summits with the surrounding semiarid climate. Their role as water providers is key in these regions during the warm and dry seasons and constitute the major when not the only water source for many rivers in the summer. Here, water fluxes from the snowpacks show a shift from the predominant partition usually found in colder and wetter climates between snowmelt and sublimation on an annual basis (Herrero and Polo, 2016), and their seasonal regime, being the radiation balance one of the responsible drivers to enhance sublimation during cold and dry periods, and intense snowmelt rates during late winter and spring (McDonell et al., 2013; Liu et al., 2019). However, weather stations are not always equipped to monitor the global radiation nor their components and, moreover, they are seldom found in high altitudes, especially over 1500 m a.s.l., which makes it difficult to accurately assess not only trends or shifts in solar radiation regimes but also the spatial patterns of solar radiation fields in high mountain areas. This impacts the availability of data for studies in mountains dealing with climate and hydrology, global warming, all the ecosystem services provided by the snow areas, and environmental and social and economical impacts on-site and downstream (Yang et al., 2010; Liu et al., 2012a; Tang et al., 2019). It is not surprising that many mountain regions are identified as biodiversity hotspots around the world, with Mediterranean and other semiarid to arid regions being highly represented (Myers et al., 2000; O'Farrell et al., 2010; Hewitt, 2011; Pauli et al., 2012).

There are several research papers on solar radiation estimations from routine observations in high altitude regions (Dubayah and van Katwijk, 1992; Dubayah, 1994; Tovar et al., 1995; Oliphant et al., 2003; Tovar-Pescador et al., 2006; Yang et al., 2006, 2010; Batllés et al., 2008; Bosch et al., 2008; Sheng et al., 2009; Aguilar et al., 2010; Mamassis et al., 2012; Chen et al., 2013). All of them insist on the need to consider topographic effects and advise against their estimation by simply interpolating or extrapolating from nearby observations. However, radiation data obtained from a dense and properly-maintained weather station network in mountainous areas are rarely available and therefore, modeling techniques need to be applied. Liu et al. (2012a) state that the most difficult issue in solar radiation modeling in data sparse regions is cloud accounting, due to the rapid spatially and temporally changing weather conditions and the three-dimensional structure of clouds. This complexity adds to the heterogeneity resulting from shadowing and reflection due to steep topography (Dubayah, 1992; Batllés et al., 2008; Mamassis et al., 2012; Chen et al., 2013).

According to Dubayah and Rich (1995), as solar radiation models become more complex, they can be more difficult to use, mainly because of the requirement for additional input data. In fact, the complexity of physically-based solar radiation formulations for topography and the lack of the data needed to drive such formulations led in the past to the lack of suitable modeling tools (Dubayah, 1994). Thus, it is important that the models allow for some flexibility with regard to the component of radiation calculated and the input data needed.

In the past decades, several models based on Geographic Information Systems (GIS) that include the topographic effects on incoming solar radiation have been proposed (e.g. Dubayah and Rich, 1995; Fu and Rich, 2000, 2002; Wilson and Gallant, 2000; Goldberg and Häntzschel, 2002; Sùri and Hofierka, 2004; Liu et al., 2012a). Required input data include digital elevation

https://doi.org/10.5194/essd-2020-250
Preprint. Discussion started: 28 October 2020

values and atmospheric attenuation parameters that are commonly estimated from ground-based measurements and/or satellite data (Dubayah, 1994).

The aim of this study was to generate the spatiotemporal distribution of global solar radiation in a high mountain semiarid area in southern Spain by means of a modeling scheme that reconstructs time map series from the usually available weather datasets. For this purpose, a GIS-based topographic solar radiation model (Aguilar et al., 2010) was applied in Sierra Nevada (Spain), a high mountain range running west-east parallely to the Mediterranean coastline with influence from both the sea and the proximity of the African continent to the South, and the continental conditions to the North. The accuracy of solar radiation estimates by the model were evaluated in terms of the error in the approximation to observed data. This study site is a high-value environmental area declared Biosphere Reserve by UNESCO in 1986 due to the exceptional presence of endemisms (Heywood, 1995; Blanca et al., 1998; Anderson et al., 2011; Cañadas et al., 2014), and included in the Global Change Observatories Network given its singular location between two seas and two continents, and its extreme topographic gradients (Bonet-García et al., 2015).

This paper presents 19 years of monthly and annual solar radiation distributed maps with high resolution (30 m x 30 m) over Sierra Nevada. The huge number of actors involved in the management of this area make this information valuable in different fields, such as: hydrology, crucial role of energy budget in the hydrological cycle over this area; ecology, ecological communities behaviour and development clearly link with the amount of energy available; production systems downstream, as hydropower facilities and traditional to tropical crop systems from the top to downhills. Besides, these data sets directly contribute, or are relevant for many studies that could do so, to two of the 23 Unsolved Problems in Hydrology (UPH) recently posed by Blöschl et al. (2019) in a participatory analytical discussion among the scientific community: UPH 16 “How can we use innovative technologies to measure surface and subsurface properties, states and fluxes at a range of spatial and temporal scales?” and UPH 5 “What causes spatial heterogeneity and homogeneity in runoff, evaporation, subsurface water and material fluxes (carbon and other nutrients, sediments), and in their sensitivity to their controls (e.g. snowfall regime, aridity, reaction coefficients)?”.

2 Study site

The Sierra Nevada mountain range (SN) is located 35 km north from the Mediterranean Sea (Fig. 1) and constitutes a mountainous area of the Natura 2000 network. Elevations rise up from 262 m a.s.l. to 3479 m a.s.l. in a 4583.72 km^2 area that runs parallel to the sea. High altitudinal gradients are representative of the area, with variation in elevation of about 3400 m in less than 40 km of horizontal distance, and a mountain climate in the summits surrounded by Mediterranean climate in the lower areas. Thus, the interaction of such conditions creates a strong heterogeneity in terms of soil types, landforms and vegetation species that determine a complex hydrological response in the area and a large number of endemic species (Heywood, 1995; Blanca et al., 1998; Anderson et al., 2011). The rainfall regime is highly variable, even in consecutive years, with annual cumulative values in the period (1960-2000) that range between 200 mm in dry years to 1000 mm in wet years,

https://doi.org/10.5194/essd-2020-250
Preprint. Discussion started: 28 October 2020

with an average value of 510 mm (Pérez-Palazón et al., 2015). Temperature regime is also heterogeneous, with values of 26, 12.5 and 0.4 ºC, for maximum, mean and minimum daily temperature in the same periodThe snow presence becomes relevant from November and above 2000 m a.s.l. The snowmelt season offset is highly variable. In general, snow is present during spring with conditions that make it possible the activity along the spring of a major ski resort in the area. However, in some years most of the snow is melt during the mild winter period episodes often found in Mediterranean climate, in January and February, significantly before the average end of the snow season in the area (Herrero et al., 2009; Herrero and Polo, 2012). Because of its singular characteristics and fragile environment, Sierra Nevada receives international recognition as a Biosphere Reserve (1986), a National Park (1999), an Important Bird Area (2003), a Special Area of Conservation (2012) and one of the International Global Change Observatories in Mountain Areas. These environmental protection figures together with the different actors involved in the management of such a unique area have determined the strong effort in data collection in the last years in order to advance in the knowledge of the different aspects that determine the dynamics of this natural system. Moreover, global warming impacts threaten the environmental values of this system but also the associated ecosystem services and social and economical activities due to the estimated shift of the snowfall regime (Pérez-Palazón et al., 2018).

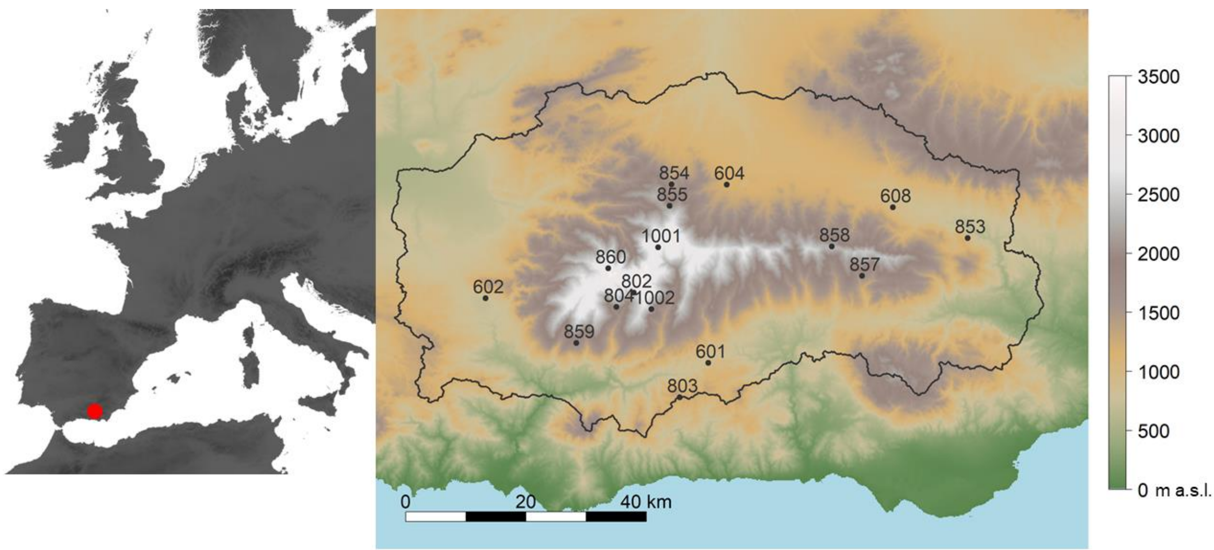

Figure 1. Location of the study site in southern Spain (left). Digital Elevation Model (DEM) and weather stations in Sierra Nevada (SN) (right).

3 Data availability

Two sources of information have been used to produce the complete solar radiation data series and maps. First, a digital elevation model (DEM) as topographic input data with 30-m spatial resolution and 1-m vertical precision (Fig. 1). The DEM is used to calculate the slope, aspect, sky view factor and terrain configuration maps that are used in the modeling process (Dozier and Frew, 1990).

Second, the longest available point information of in situ daily global radiation (R_{go}) measured in 16 weather stations over the area (Fig. 1 and Table 1). The extent of the records in all weather stations (N_o in Table 1) was considered long enough to carry out the evaluation process dating from February 2000 for the oldest station (608 in Table 1). 12 out of the 16 weather stations are located above 1500 m a.s.l. and 7 of them above 2000 m a.s.l. (Fig. 1). The stations belong to four different organizations: the Department of Agriculture, Fisheries and Environment of the Andalusian Government (601-608 in Table 1), the Water and Environment Agency (1001 and 1002 in Table 1), the National Parks Organization (853-860 in Table 1) and the Guadalfeo Network (802-804 in Table 1) described in Polo et al. (2019). Pyranometers used to collect the data were of different natures but all of them with a characteristic range of around 0.35 ~ 1.1 μm: Skye SP1110 (stations 601, 602, 604 and 608), Kipp & Zonen SP-Lite pyranometer (station 802), HuksefluxLP02 (station 803), HuksefluxNR01 (stations 1001, 1002 and 804) and Middleton Net Solar CNR1 (stations 853, 854, 855, 857, 858, 859 and 860).

In order to generate the complete global radiation data series for the whole time span (01/02/2000-31/12/2018) we first apply a quality-control check to recorded data at the weather stations in terms of standard limit checking, as well as the implementation of a particular test to discard undetected suspicious data due to singularities often found in high altitudes.

3.1 Data quality control

Numerous studies on quality control of measured solar radiation data can be found in the literature (Geiger et al., 2002; Younes et al., 2005; Moradi, 2009; Journée and Bertrand, 2011). Compared to other meteorological variables, solar radiation measurement is more prone to errors (Moradi, 2009). Younes et al. (2005) state two main sources of errors related to in situ measurement of solar radiation: those related to equipment and uncertainty and operational errors. Thus, previous to any computation two logical tests were applied to recorded daily global radiation data to discard suspicious records associated with equipment and operational errors (Younes et al., 2005).

1. Observed daily global radiation (R_{go}) must be between the daily extraterrestrial radiation (R_{ext}) and a minimum 3% of R_{ext} (Geiger et al., 2002; Moradi, 2009).
2. Observed daily global radiation (R_{go}) must be lower than the clear daily global radiation (R_{gcs}) observed under a highly transparent clear sky (Wu et al., 2007). R_{gcs} values were modelled with the expression of Ineichen and Perez (2002) and the parameterization of Kasten and Young (1989) for the air mass.

The excluded values from these tests did not reach 1% of the data at any weather station.

A third quality control was applied following Younes et al. (2005) to undetected suspicious data expected to be erroneous due to the particularities of weather stations in high altitudes (e.g. shadows, impacts of snow, mechanical failures, etc.). They suggest the creation of an expectancy envelope in the clearness index (CI)-diffuse to global irradiance ratio (k) domain to

https://doi.org/10.5194/essd-2020-250
Preprint. Discussion started: 28 October 2020

Open Access Earth System Science Data Discussions

remove R_{go} data too obviously erroneous. After this quality test, the percentage of excluded values did not reach 10% at any weather station, with a mean value close to 2% when the whole set of stations was considered. Table 1 shows selected descriptors of the data sets at each station in this study after all the quality check process.

Table 1. Information of the weather stations included in this study: elevation, z (m a.s.l.); code; data length, as initial and final dates of the time series; number of initially available daily records, N_o (days); number of available daily records after the quality check, N (days); rate of days for cloudy, $N_{CI<0.3}$ (%), partially cloudy, $N_{0.3<CI<0.6}$ (%), and clear-sky conditions, $N_{CI>0.6}$, (%); and maximum, R_{go_max} (MJ m^{-2} day^{-1}), mean, R_{go_mean} (MJ m^{-2} day^{-1}), and minimum, R_{go_min} (MJ m^{-2} day^{-1}), daily global radiation observed values. The selected descriptors for sky conditions and global radiation correspond to registered data after quality check.

z	Code	Initial date	Final date	N_o	N	$N_{CI<0.3}$	$N_{0.6<CI<0.3}$	$N_{CI>0.6}$	R_{go_max}	R_{go_mean}	R_{go_min}
3097	860	23/01/2008	09/09/2018	1858	1705	13	25	62	35.79	18.20	1.12
2867	1001	16/11/2007	01/01/2014	1071	1071	6	28	66	33.70	18.06	1.68
2510	802	04/11/2004	31/12/2018	5050	4849	6	19	75	36.29	20.28	0.69
2325	1002	15/11/2008	29/10/2012	951	951	8	22	70	35.60	20.47	1.55
2300	858	09/03/2008	20/09/2017	2385	2380	12	28	60	34.58	17.99	0.99
2155	855	02/01/2008	30/11/2017	2522	2519	13	30	57	33.64	17.64	0.78
2141	804	10/10/2012	31/12/2018	2272	2206	7	21	72	33.91	19.05	0.82
1735	859	23/01/2008	21/11/2018	2577	2573	11	23	66	33.67	19.11	0.59
1732	857	16/11/2007	29/12/2018	3042	3034	11	25	64	32.84	18.31	0.81
1530	854	26/10/2007	16/12/2018	3176	3169	10	28	62	32.91	17.97	1.10
1332	803	27/08/2009	31/12/2018	3407	3282	7	22	71	33.41	18.95	0.71
1212	604	05/09/2000	31/12/2018	6665	6485	7	29	64	33.00	18.09	0.70
975	853	21/11/2007	29/12/2018	2833	2827	8	30	62	32.37	18.01	1.00
950	601	05/09/2000	31/12/2018	6600	6449	7	27	66	33.00	18.17	0.60
942	608	01/02/2000	31/12/2018	6883	6686	6	26	68	34.20	18.83	0.70
781	602	26/01/2001	31/12/2018	6521	6370	8	23	69	33.80	18.49	0.80

3.2 Generation of missing daily global radiation data at weather stations

From the chronogram (Figure 2) of the data availability per station (N in Table 1), gaps of different nature are visible along the study period. There are two kinds of gaps: those associated with the installation of the weather station (determined by the initial and final dates indicated in Table 1), and those within the datasets that are due to operational issues such as equipment errors, maintenance labors, etc. The latter were removed in the quality control check.

https://doi.org/10.5194/essd-2020-250
Preprint. Discussion started: 28 October 2020

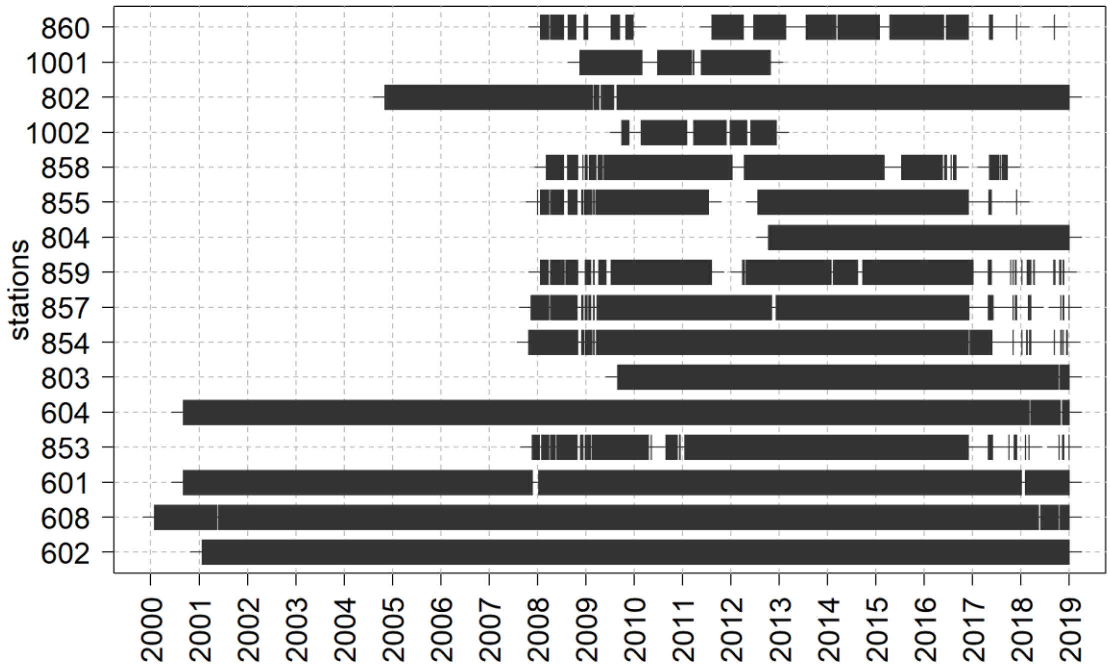

Figure 2. Data availability in the analyzed period (01 Feb 2000 - 31 Dec 2018) for each weather station. Stations are sorted by increasing altitude.

In order to fill all these gaps at each weather station, the model proposed by Aguilar et al. (2010) that was previously implemented and validated in a small subwatershed located in the southwest of Sierra Nevada (Fig. 1) was extended to the whole area in this study. In this study the records obtained from weather stations are considered to represent the average values of the cell on which they are located despite they constitute a point source of information following the assumptions of previous studies that deal with distributed data (Batllés et al., 2008; Martínez-Durbán et al., 2009).

The main equations and flowchart of the model are shown in Appendix A. The complete explanation of the algorithms as well as the justification of the assumptions of the model can be found in detail in Aguilar et al. (2010).

The model was developed to be run using limited data but considering the agents that constitute the main sources of the spatial and temporal variability of solar radiation. Results generated by the model include hourly maps of diffuse, beam and reflected solar radiation values with minimum input data requirements as only topographic data and measured daily global radiation records (R_{go}) at least at one weather station are required. Regarding topographic data, if unavailable, free satellite-based digital elevation models can be used (e.g. GMTED2010, GTOPO30 by NASA). As for the daily global radiation registers, even when they are missing, their estimation from other more readily available meteorological data could always be a choice from the literature (Hargreaves and Samani, 1982; Bristow and Campbell, 1984; Allen, 1997; Bechini et al., 2000; Winslow et al., 2001;

https://doi.org/10.5194/essd-2020-250
Preprint. Discussion started: 28 October 2020

Donatelli et al., 2003, 2006; Yang and Koike, 2005; Diodato and Bellocchi, 2007; Wu et al., 2007; Ruiz-Arias et al., 2011; Liu et al., 2012b; El Ouderni et al., 2013; Mullen et al., 2013).

Once daily global radiation estimates were generated by the model a cross validation was applied at each weather station on the daily scale. This was carried out on a leave-one-out process, i.e. data from a weather station were removed from the input dataset to the model and predicted values (R_{gp}) at that weather station were then compared to observed data (R_{go}).

Different indicators were computed to quantitatively evaluate the performance of the model (Muneer et al., 2007):

-The Root Mean Square Error (RMSE) (Eq. 1), where R_{gp} and R_{go} are the predicted and observed daily global radiation (MJ m^{-2} day^{-1}), respectively, and N the number of observed daily data. It gives a value of the level of scatter by the model as it provides the comparison term-by-term of the actual deviation between the estimated and the measured values.

$$RMSE = \sqrt{\frac{\sum\left(R_{gp} - R_{go}\right)^2}{N}} \tag{1}$$

-The deviation from the 1:1 line of observed vs. predicted daily solar radiation values. Linear fits forced through the origin were obtained (Eq. 2) and the slopes (α in Eq. 2) are desired to be equal to 1. The coefficient of determination, R^2, as the ratio of the explained variation to the total variation, was also computed.

$$R_{gp} = \alpha \cdot R_{go} \tag{2}$$

The RMSE values and linear fits were obtained for the whole dataset at each weather station, and also for different cloudiness levels to consider different atmospheric states that may condition the performance of the model according to previous studies (Batllés et al., 2008; Martínez-Durbán et al., 2009; Ruiz-Arias et al., 2009). Three atmospheric states were analyzed: cloudy days ($CI<0.3$), partly cloudy days ($0.3 \leq CI < 0.6$) and clear-sky days or cloudless days ($CI \geq 0.6$).

3.3 Generation of daily global radiation maps at the study site

The generation of distributed global radiation data with the model applied (Aguilar et al., 2010) requires a proper characterization of the spatio-temporal patterns of albedo in the study site. 240 cloud-free Landsat imagery available for the study period from Landsat 5 TM (49 images), Landsat 7 ETM+ (141 images) and Landsat 8 OLI (50 images) were used. All images were first properly corrected and their reflectivity values computed (Pimentel et al., 2014). Albedo was then derived for each image following the same procedure applied in Aguilar et al. (2010), which is based on the methodology described by Brest and Goward (1987), and linearly interpolated on a daily time scale for the whole study period.

4 Daily data series at weather stations

First, the evaluation of the predicted global radiation daily series is applied and then the final filled daily data series are provided at each weather station.

4.1 Cross-validation

The cross-validation assessment is summarized in Figure 3. With the global datasets (in black in Fig. 3), a very close approximation of the model estimates to recorded data was obtained (mean α value of 0.98 and mean R^2 values of 0.91). RMSE values varied for the different stations and ranged from 1.81 (station 804) to 3.76 (station 860) with a mean value of 2.63 MJ m^{-2} day^{-1}. These errors are within the order of magnitude of those found in previous studies in other mountainous areas (Yang et al., 2006; 2010) as well as in the north-eastern side of SN (Tovar-Pescador et al., 2006; Batllés et al., 2008; Ruiz-Arias et al., 2009).

When the analysis was carried out in terms of the cloudiness level, a general overestimation by the model (e.g. a mean α value of 1.41) was always seen on cloudy days (CI≤0.3). In contrast, on clear-sky days (CI>0.6) slopes were very close to 1 with a mean α value of 0.96. An intermediate behavior was found on partly cloudy days (0.3<CI≤0.6) when the model slightly under predicted (e.g. stations 854 and 608) or over predicted depending on the weather station. As for RMSE values, the lowest values were always found for clear sky days, when the cloud influence is minimal and the attenuation is mostly explained by changes in the atmospheric transmittance, followed by partly cloudy days with mean values of 2.07 and 3.07 MJ m^{-2} day^{-1}, respectively. The highest RMSE values were always found on cloudy days with mean values of 3.70 MJ m^{-2} day^{-1}. The high proportion of clear-sky days (65%) and the low RMSE values on these days (2.07 MJ m^{-2} day^{-1}) revealed the general good agreement of the model estimates with observed data. This is especially important in semiarid environments, where energy-limited hydrological processes (e.g. soil moisture depletion, evaporation or snowmelt) are more relevant on clear-sky days and they must be carefully computed in water and energy balance modeling, irrigation scheduling, etc. (Chen et al., 1999; Mamassis et al., 2012).

https://doi.org/10.5194/essd-2020-250
Preprint. Discussion started: 28 October 2020

Open Access Earth System Science Data Discussions

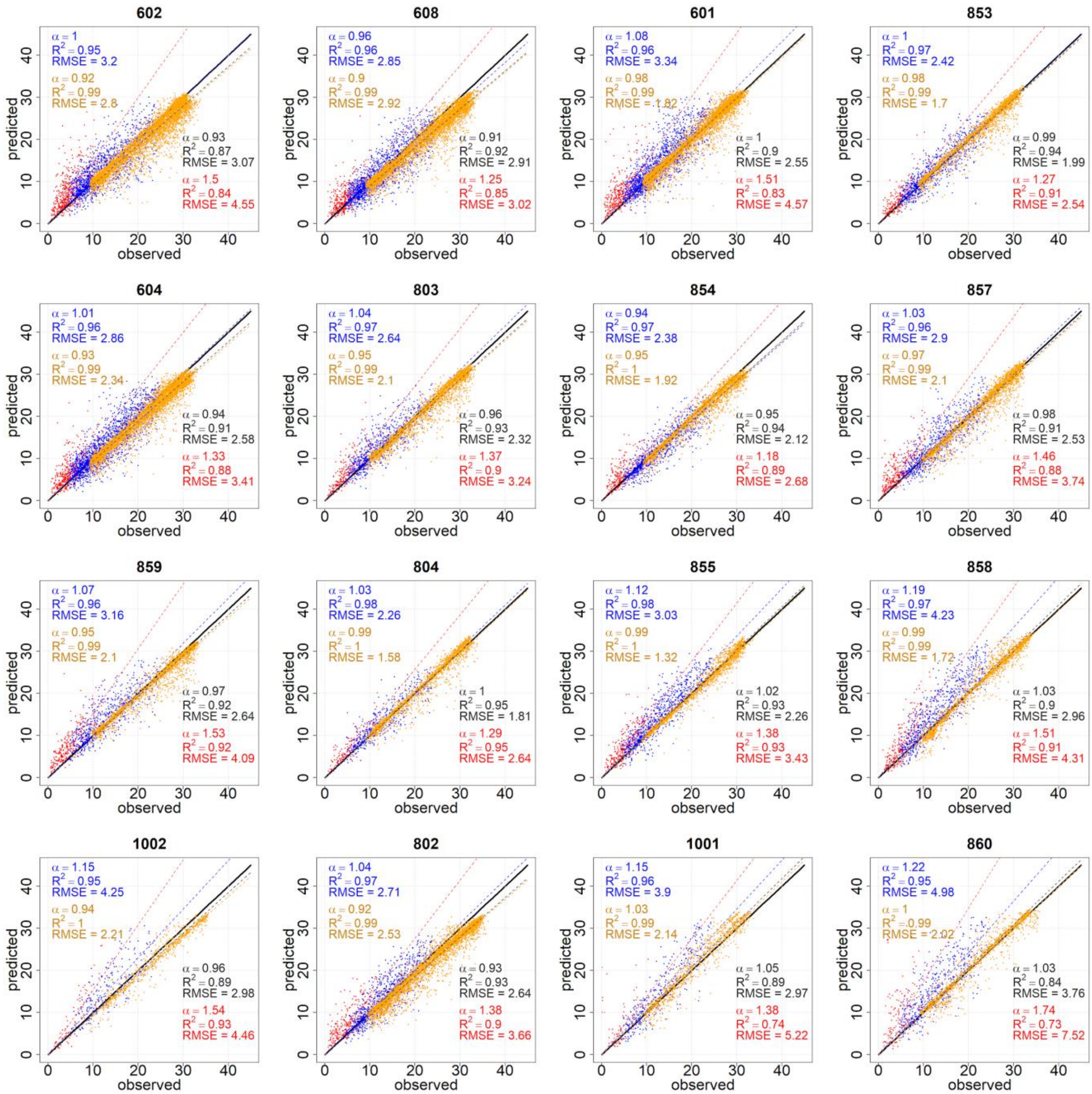

Figure 3. Cross validation analysis. Linear fits of daily predicted *vs.* observed R_g (MJ m^{-2} day^{-1}) at each one of the selected stations for the global data (black), cloudy (CI<0.3 - red), partly cloudy (0.3<CI<0.6 - blue) and clear-sky days (CI>0.6 - orange). Stations are sorted by increasing altitude.

https://doi.org/10.5194/essd-2020-250
Preprint. Discussion started: 28 October 2020

Considering the elevation of the stations, there is no clear pattern as the goodness of the model estimates was more affected by the spatial configuration of the weather stations network with available data than by the height of the station itself. Obviously, the closest a station with available records is to a certain location, the better the estimates of cloudiness and therefore, the daily predicted R_g value.

4.2 Filled time series

Figure 4 shows the distribution of the daily filled R_g in each weather station sorted by altitude and illustrates several questions already appreciated in the observed series (Table 1): i) a quite stable minimum daily R_g around 1 MJ m^{-2} day^{-1} and a very similar interquartile range among stations, ii) greater variations in the maximum daily R_g among the different stations with a mean value of 34.0 MJ m^{-2} day^{-1}, and iii) even though a slight increase with altitude can be appreciated in the high extreme statistics of the daily filled R_g values, such as the maximum and the 90th percentile, there is not a clear trend and other factors such as orientation, proximity to the sea or the terrain configuration in the surrounding terrain constitute relevant features.

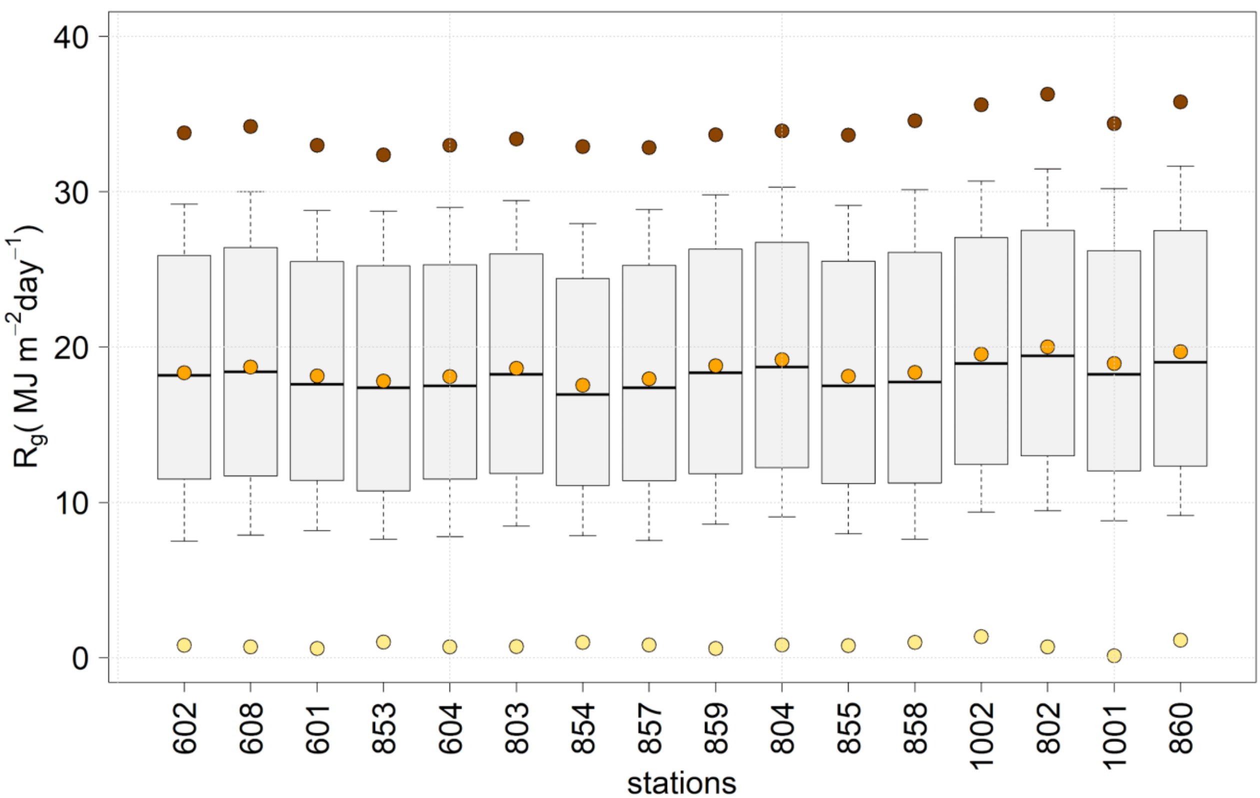

Figure 4. Distribution of filled daily R_g (MJ m^{-2} day^{-1}) time series in each of the selected stations over the study area. The box shows 50% of the data, delimited by Q1 (lower) and Q3 (upper), the solid line represents the median, and whiskers show 10th and 90th

https://doi.org/10.5194/essd-2020-250
Preprint. Discussion started: 28 October 2020

percentiles. Brown, orange and yellow dots represent daily maximum, mean and minimum time series values. Stations are sorted by increasing altitude.

5 Monthly time series of global radiation in Sierra Nevada

The monthly distribution of the filled R_g series per weather station (Fig. 5) shows that in every station: i) July and December constitute the months with the highest and the lowest values of R_g, respectively; ii) there is a quite linear increase in the monthly R_g values from January to July and a sudden drop in August with a curved evolution till December; and iii) the interquartile range is significantly higher in the spring and fall, than in the summer and winter months.

The increase in the high extreme statistics of radiation with the altitude of the weather station becomes more apparent at the monthly scale (Fig. 5) than at the daily scale (Fig. 4) previously analyzed. Thus, maximum values of around 1000 MJ m^{-2} $month^{-1}$ are reached in July in the highest stations (e.g. 1002, 802, 1001 and 860 in Fig. 5) whereas this value decreases to around 910 MJ m^{-2} $month^{-1}$ in the four lowest stations with the exception of station 608.

The monthly distributed R_g time series show significant spatial differences of up to 200 MJ m^{-2} $month^{-1}$ in both the mean monthly values (Fig. 6) and the rest of the statistics (Fig. 7), that clearly follow the terrain configuration with summits and valleys receiving high and low solar radiation values, respectively. For example, the area in the north of SN that is highly shadowed by the highest peaks in the Iberian Peninsula (Mulhacen and Veleta with 3482 and 3396 m a.s.l., respectively) is easily visible, with the lowest relative levels of insolation received within SN especially in the summer months (June, July and August in Fig. 6).

Both, maps of the monthly mean and standard deviation of R_g (Fig. 6) and the monthly distribution of R_g in the study site (Fig. 7), allow to draw the same conclusions as those previously obtained in the monthly values per weather station regarding: i) July and December as the months with the highest and lowest values of R_g received in SN; and ii) the highest dispersion in the monthly R_g values in the spring and fall months.

For the study period (2000-2018), there is a great heterogeneity in the monthly distribution of R_g at the study site (Fig. 7) especially in the incoming radiation along the months of the wet season. In this way, in the most insolated years in the study period (2005 and 2012), significantly higher monthly radiation values were found in certain months of the spring time (March and May 2012 and April 2005). In those months, the higher than usual rate of clear-sky over cloudy days finally determines the annual differences in the incoming global radiation in SN.

When considering the temporal evolution of the monthly distribution of R_g in SN (Fig. 8), certain interannual differences can be observed along the study period, such as the existence of certain months in spring with unexpected low monthly radiation values (eg. 2001, 2004, 2007 and 2008), or two relative maximum monthly R_g values (e.g. 2009, 2010 and 2014). Moreover, Figure 8 shows a higher dispersion in the monthly maximum (June-August) and minimum (November-January) R_g values in SN than when the analysis is carried out at each weather station (Fig. 5).

https://doi.org/10.5194/essd-2020-250
Preprint. Discussion started: 28 October 2020

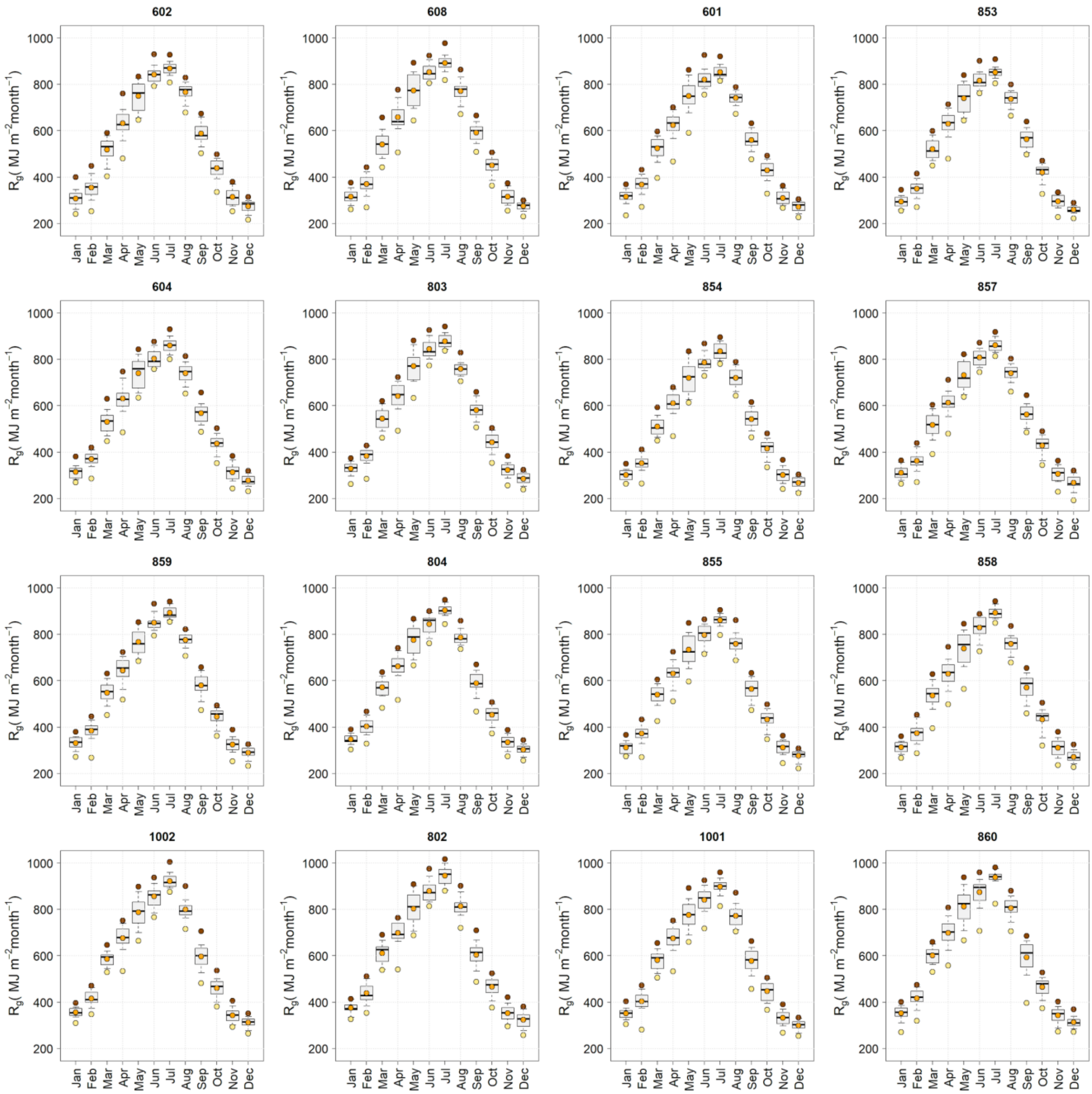

Figure 5. Monthly distribution of filled daily R_g (MJ m^{-2} month^{-1}) time series in each of the selected stations over the study area. The box shows 50% of the data, delimited by Q1 (lower) and Q3 (upper), the solid line represents the median, and whiskers show 10th and 90th percentiles. Brown, orange and yellow dots represent monthly maximum, mean and minimum time series values. Stations are sorted by increasing altitude.

https://doi.org/10.5194/essd-2020-250
Preprint. Discussion started: 28 October 2020

Earth System Science Data
Open Access Discussions

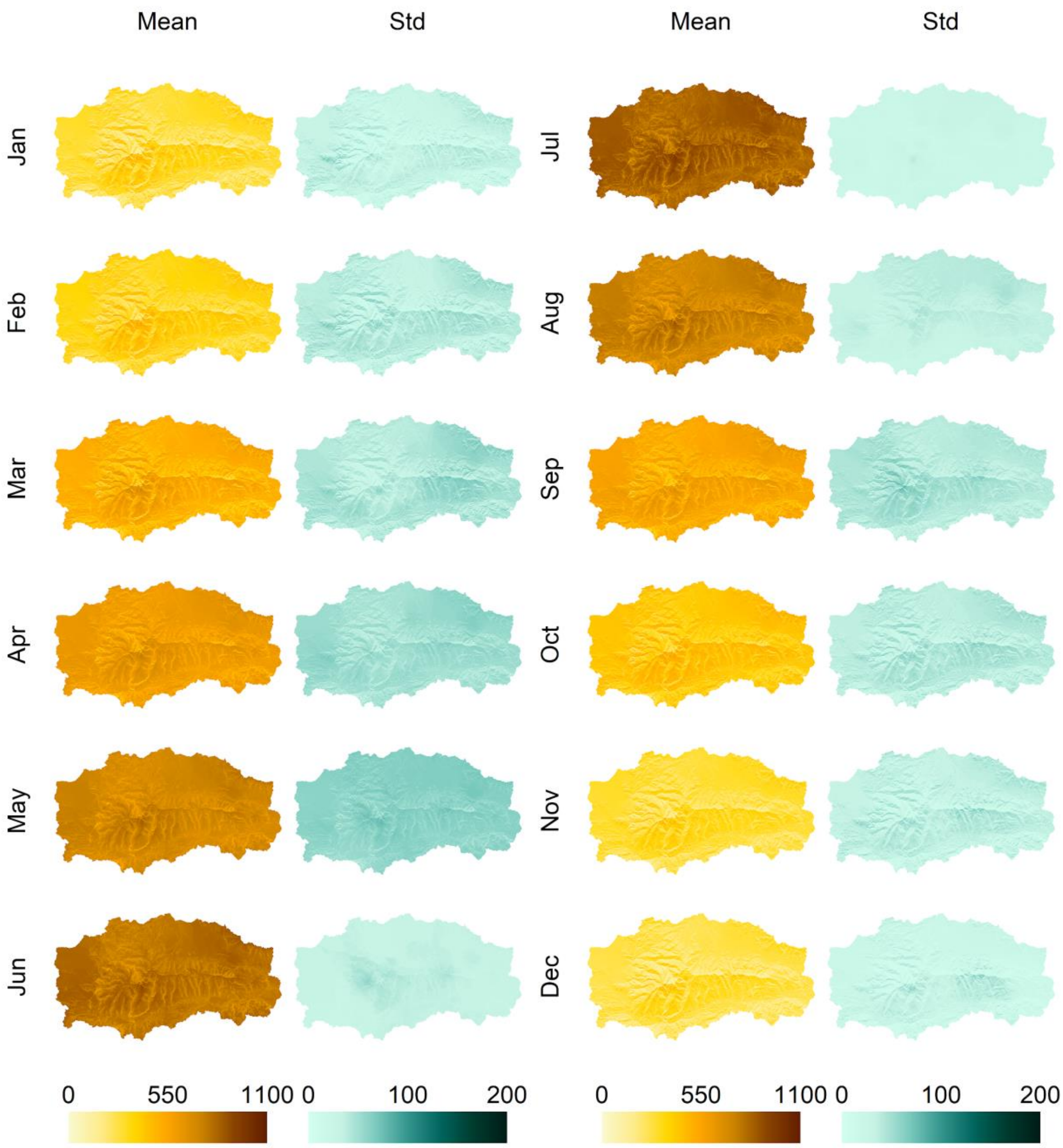

Figure 6. Monthly average and standard deviation of R_g (MJ m^{-2} month^{-1}) in the study period (2000-2018) in SN.

https://doi.org/10.5194/essd-2020-250
Preprint. Discussion started: 28 October 2020

Open Access Earth System Science Data Discussions

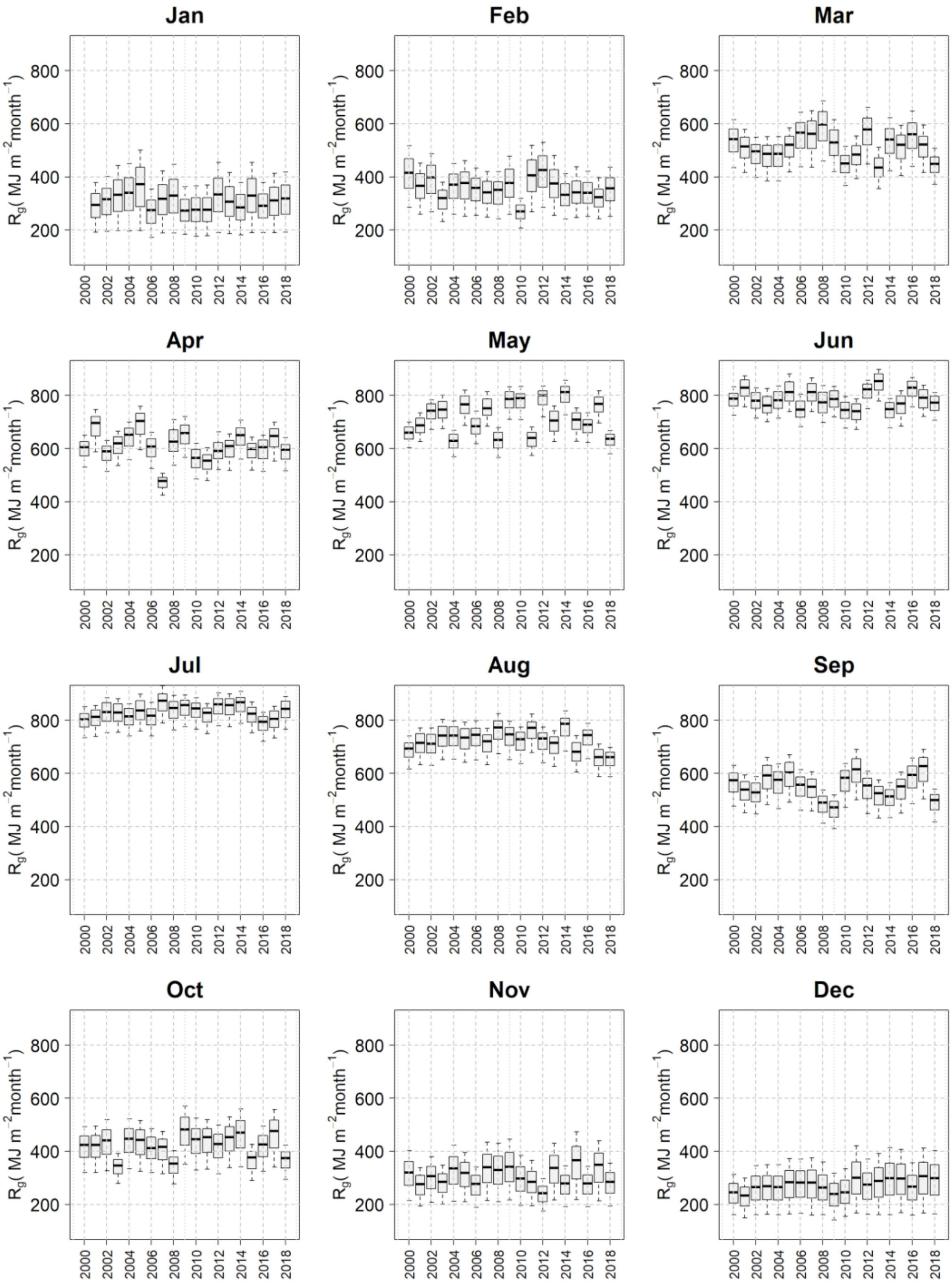

282

283 **Figure 7. Monthly distribution R_g (MJ m^{-2} month^{-1}) in the study period (2000-2018) in the whole area of SN.**

284

https://doi.org/10.5194/essd-2020-250
Preprint. Discussion started: 28 October 2020

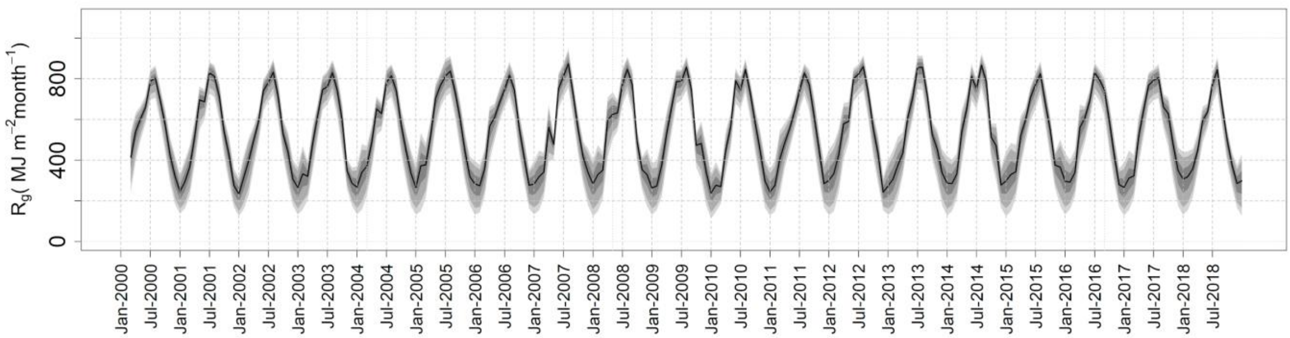

Figure 8. Evolution of the distribution of monthly R_g (MJ m^{-2} month^{-1}) in the study period (2001-2018) in the whole area of SN.

6 Annual times series of global radiation in Sierra Nevada

Unlike at the daily scale (Fig. 4), a great variability among the different weather stations in terms of the global radiation received at the annual temporal scale is found (Fig. 9). Thus, we find minimum annual R_g values from 5920 MJ m^{-2} year^{-1} in station 854 to around 6750 MJ m^{-2} year^{-1} in station 1002. This difference is even bigger in the maximum annual R_g values from 6700 to 7720 MJ m^{-2} year^{-1} in stations 854 and 802, respectively, and is also appreciated in the interquartile range.
When analyzing the influence of altitude, the weather stations above 1500 m a.s.l (854, 857, 859, 804, 855, 858, 1002, 802, 1001, 860 in Fig. 9) show their altitudinal gradient in all the statistics of the annual R_g values considered.

The annual distributed time series (Fig. 10) show the same spatial differences that follow the terrain configuration as those observed in the monthly time series (Fig. 6). For example, the area in the north of SN that is highly shadowed as previously mentioned corresponds to the area with the mean minimum annual values received in the study period, 4063 MJ m^{-2} year^{-1}, that only represents 63% the mean annual accumulated values in SN (6316 MJ m^{-2} year^{-1}).

Significant interannual differences can be easily appreciated with differences in the mean annual R_g value in the study area of up to 800 MJ m^{-2} year^{-1} between 2005 and 2018. Such years with particularly high and low annual incoming radiation also presented higher (6800 MJ m^{-2} year^{-1}) and lower median annual R_g values (6200 MJ m^{-2} year^{-1}), respectively, than the annual median for the whole study period in SN (6456 MJ m^{-2} year^{-1}) (Fig. 11). These results agree with the annual irradiation map obtained by Batllés et al. (2008) in the north-eastern part of SN. They reported maximum and minimum annual values of 7516 and 2342 MJ m^{-2} year^{-1} on the summits and in deep valleys, respectively, and thus, concluded that irradiation levels were more related to topographic characteristics than to altitude.

https://doi.org/10.5194/essd-2020-250
Preprint. Discussion started: 28 October 2020

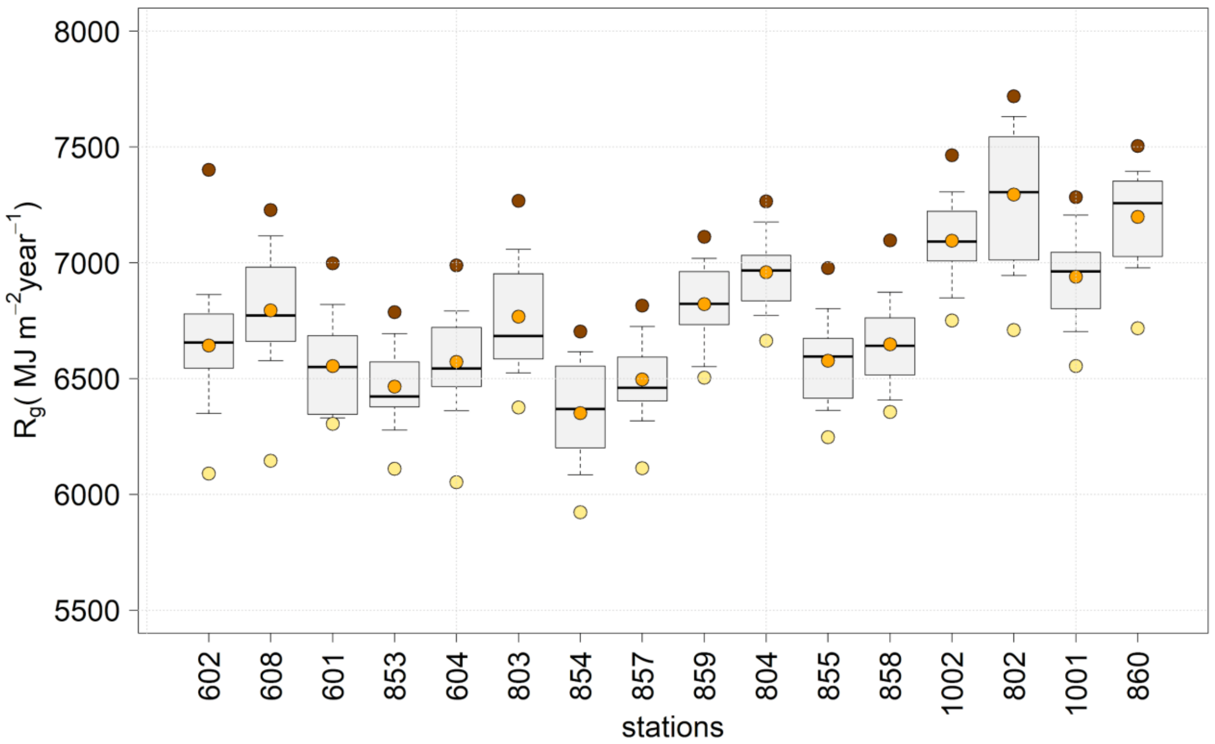

Figure 9. Annual distribution of filled daily R_g (MJ m^{-2} year^{-1}) time series in each of the selected stations over the study area. The box shows 50% of the data, delimited by Q1 (lower) and Q3 (upper), the solid line represents the median, and whiskers show 10th and 90 th percentiles. Brown, orange and yellow dots represent annual maximum, mean and minimum time series value.

https://doi.org/10.5194/essd-2020-250
Preprint. Discussion started: 28 October 2020

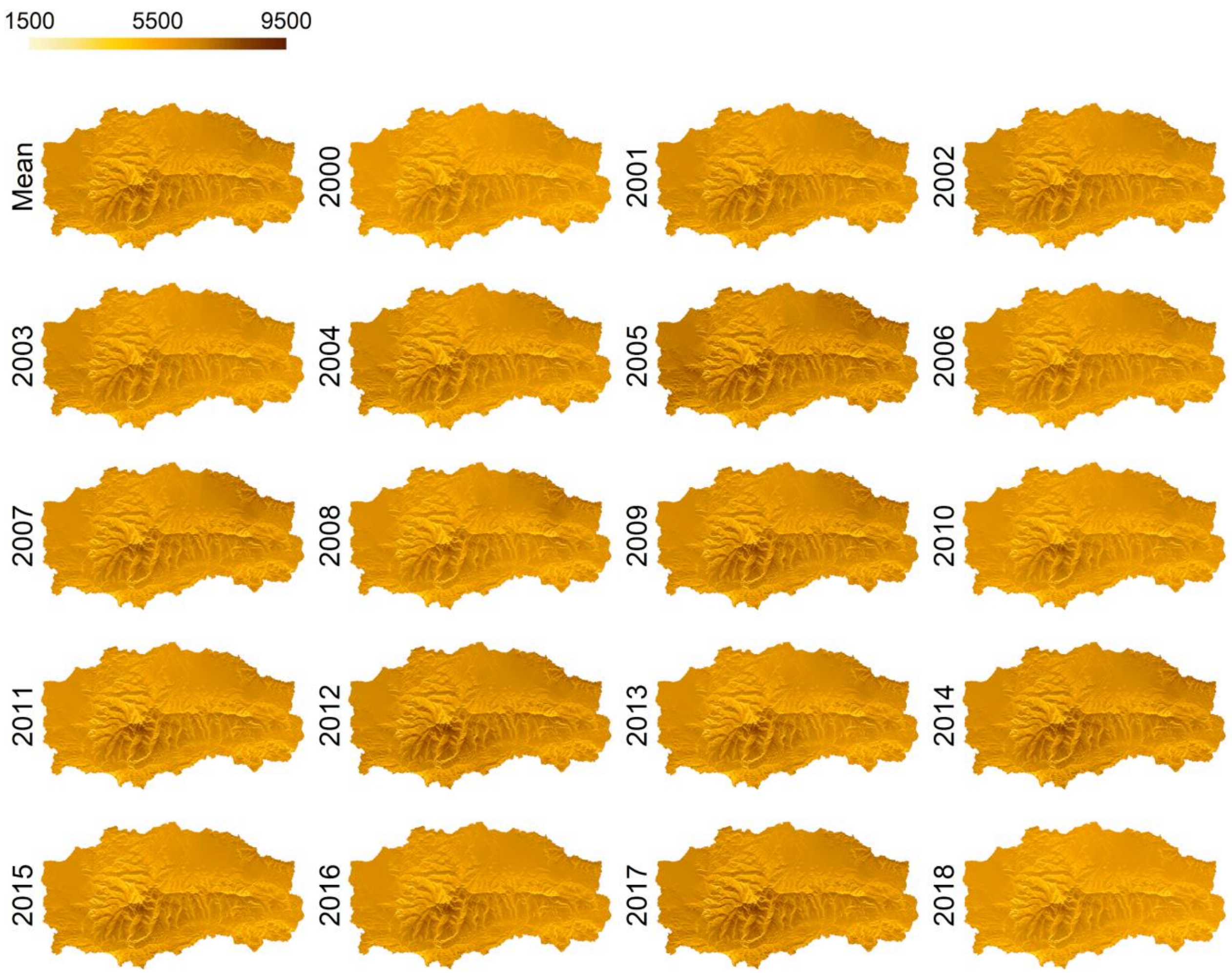

Figure 10. Annual global radiation (MJ m^{-2} year^{-1}) in the study period (2001-2018) in SN.

https://doi.org/10.5194/essd-2020-250
Preprint. Discussion started: 28 October 2020

Open Access Earth System Science Data Discussions

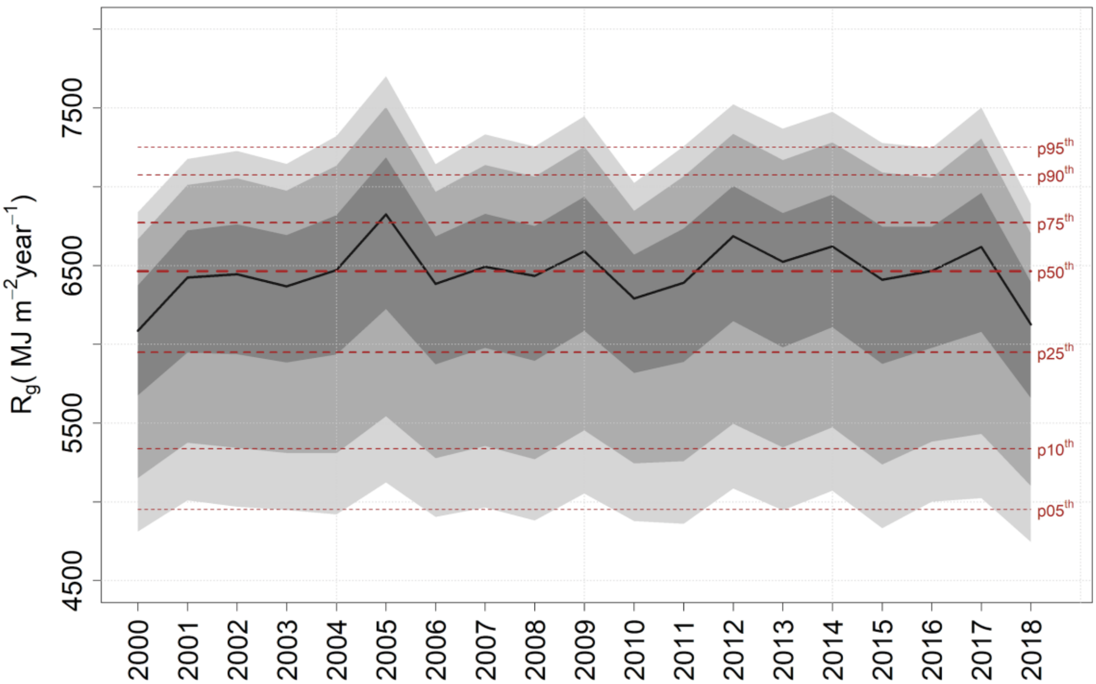

Figure 11. Evolution of the distribution of annual R_g (MJ m^{-2} year^{-1}) in the study period (2001-2018) in the whole area of SN. In dashed lines the mean values in the study period of the different percentiles shown in the global distribution for this period.

7 Data applications for research and operational capabilities

Time series of the surface global radiation datasets can be used to analyze trends, inter-annual and seasonal variation characteristics of the global radiation received in SN with high spatial detail (30 m). The availability of long global radiation datasets allows to capture the multi-year periodicities in the sun's activity cycle continuously reported in the literature (Scaffetta and Wilson, 2013) and the quantification of its influence as climate change forcing agent in these semiarid mountainous areas. Additionally, they can also be used as cross-validation reference data for other global radiation distributed datasets generated in SN with different spatio-temporal interpolation techniques.

These datasets can also be useful to assess changes in global radiation associated to different phenomena such as altitudinal/slope/aspect gradients, large scale atmospheric processes, etc., in other mountainous areas with Mediterranean-type climate conditions and limited radiation station-based observations.

The correct assessment of trends and shifts in the solar radiation regime is crucial to correctly determine the temporal evolution of energy-limited hydrological processes such as the snow layer dynamics, soil moisture depletion and evapotranspiration (Tomas-Burguera et al., 2019). Thus, as a key input parameter for the water and energy balance, these high spatial resolution

https://doi.org/10.5194/essd-2020-250
Preprint. Discussion started: 28 October 2020

solar radiation time series are useful not only for research on the snow domain and water planning in SN in the application of hydrological modelling, but also in other application areas such as the agricultural sector in their estimations of evapotranspiration for irrigation scheduling, ecology and biodiversity studies, stand-alone solar energy facilities designing and location, or recreational activities in the area that strongly rely on the hydro-meteorological conditions of SN. Finally, this work contributes to feed research related to some key questions in hydrology, as UPH 16 and UPH 5 identified by Blöschl et al. (2019).

8 Data availability

The monthly and annual global radiation maps derived in this study can be accessed and downloaded in .ncdf format from: https://doi.pangaea.de/10.1594/PANGAEA.921012 (Aguilar et al., 2020).

9 Final remarks

This study presents nineteen years (2000-2018) of monthly and annual global radiation maps of high spatial resolution (30m x 30m) in a high mountain Mediterranean site. In these areas the common lack of weather stations in high altitudes makes it difficult to accurately assess trends or shifts in solar radiation spatial patterns.

A modelling scheme based on measurements or estimations of incoming daily global radiation was applied and validated in the sixteen weather stations available at this unique study site. Mean RMSE values ranged from 1.81 to 3.76 MJ m^{-2} day^{-1}, depending on the weather station. The best estimations were always obtained on clear-sky days, when mean RMSE values decreased to 2.07 MJ m^{-2} day^{-1}. The largest errors were obtained on cloudy days, which constitute on average 10% of the daily datasets, and, therefore, future research should be conducted in order to improve the estimations in these situations keeping the minimum input data requirements (daily global radiation data) advantage of the model. However, the high proportion (65%) of clear-sky days, and the low RMSE values on those days, allow one to conclude that there is a good agreement between the model estimates and observed data in the study site.

Spatial differences of around 2000 MJ m^{-2} yr^{-1} were found within each year analyzed. In addition, significant differences were easily noted between the years in mean incoming values of up to 800 MJ m^{-2} yr^{-1}. Those differences were mostly due to the variability in the incoming radiation at the wet season (September-May), with higher rates of clear-sky days in the most insolated years (e.g. 2005).

Thus, we can affirm that the modeling scheme here applied is an efficient option in semiarid mountainous areas, where daily global radiation datasets constitute the only source of solar radiation data. This methodology could be really helpful in climate change assessment studies in other similar conditions in terms of topographic features all over the world.

Author contributions

CA, in collaboration with MJP, conceived the research. CA processed the data, applied the quality control to the raw global radiation data, modelled global radiation datasets and developed the cross-validation algorithms. RP processed satellite data, generated albedo maps for the study period, prepared the final figures and the available datasets generated in the study. CA prepared the manuscript with contributions of MJP and RP; all authors discussed and revised the final text.

Competing interests

The authors declare that they have no conflict of interest.

Acknowledgements

This study was supported by the following research projects funded by Spanish Ministry of Science and Innovation - MICINN: Research Project RTI2018-099043-B-I00, "Operability in hydrological management under snow torrentiality/drought conditions in high mountain in semiarid watersheds"; and, by Spanish Ministry of Economy and Competitiveness - MINECO: Research Project CGL 2014-58508R, "Global monitoring system for snow areas in Mediterranean regions: trends analysis and implications for water resource management in Sierra Nevada", and Research Project CGL 2011-25632, "Snow dynamics in Mediterranean regions and its modelling at different scales. Implication for water management". Moreover, the present work was partially developed within the framework of the Panta Rhei Research Initiative of the International Association of Hydrological Sciences (IAHS) (Working Groups Water and energy fluxes in a changing environment and Mountain Hydrology). Rafael Pimentel acknowledges fundings by the modality 5.2 of the *Programa Propio-2018* of the University of Cordoba and the *Juan de la Cierva Incorporación* Programme of the Ministry of Science and Innovation (IJC2018-038093-I). The continuous support of the Natural and National Park of Sierra Nevada has also been determinant for the development of this line of research since 2002. Finally, tremendous appreciation is extended to all the weather station networks that maintain and make accessible datasets to scientific research.

References

Aguilar, C. and Polo, M. J.: Generating reference evapotranspiration surfaces from the Hargreaves equation at watershed scale, Hydrol. Earth Syst. Sci., 15, 2495-2508, https://doi.org/10.5194/hess-15-2495-2011, 2011.

Aguilar, C., Herrero, J., and Polo, M. J.: Topographic effects on solar radiation distribution in mountainous watersheds and their influence on reference evapotranspiration estimates at watershed scale, Hydrol. Earth Syst. Sci., 14, 2479–2494, https://doi.org/10.5194/hess-14-2479-2010, 2010.

Aguilar, C., Pimentel, R., and Polo, M. J.: Time series of distributed global radiation data in Sierra Nevada (Spain) at different scales from historical weather stations, PANGAEA, https://doi.pangaea.de/10.1594/PANGAEA.921012, 2020.

Allen, R.G.: Self-calibrating method for estimating solar radiation from air temperature, J. Hydrol. Eng., 2, 56-67, https://doi.org/10.1061/(ASCE)1084-0699(1997)2:2(56), 1997.

Anderson, R. S., Jiménez-Moreno, G., Carrión, J. S., and Pérez-Martínez, C.: Postglacial history of alpine vegetation, fire, and climate from Laguna de Río Seco, Sierra Nevada, southern Spain, Quaternary Sci. Rev., 30, 1615–1629, https://doi.org/10.1016/j.quascirev.2011.03.005, 2011.

Batllés, J., Bosch, J.L., Tovar-Pescador, J., Martínez-Durbán, M., Ortega, R., and Miralles, I.: Determination of atmospheric parameters to estimate global radiation in areas of complex topography: Generation of global irradiation map, Energy Convers. Manage., 49, 336-345, https://doi.org/10.1016/j.enconman.2007.06.012, 2008.

Bechini, L., Ducco, G., Donatelli, M. and Stein, A.: Modelling, interpolation and stochastic simulation in space and time of global solar radiation, Agric. Ecosyst. Environ., 81, 29-42, https://doi.org/10.1016/S0167-8809(00)00170-5, 2000.

Blanca, G., Cueto, M., Martínez-Lirola, M. J., and Molero-Mesa, J.: Threatened vascular flora of Sierra Nevada (Southern Spain), Biological Conservation, 85(3), 269-285, doi:10.1016/S0006-3207(97)00169-9, 1998.

Blöschl, G. et al.: Twenty-three unsolved problems in hydrology (UPH) – a community perspective, Hydrol. Sci. J., 64 (1), 1141-1158, https://doi.org/10.1080/02626667.2019.1620507, 2019.

Bonet-García, F.J., Pérez-Luque, A.J., Moreno-Llorca, R.A., Pérez-Pérez, R., Puerta-Piñero, C., and Zamora, R.: Protected areas as elicitors of human well-being in a developed region: a new synthetic (socioeconomic) approach, Biol. Conserv., 187 221-9, https://doi.org/10.1016/j.biocon.2015.04.027, 2015.

Bosch, J.L., López, G., and Batlles, F.J.: Daily solar irradiation estimation over a mountainous area using artificial neural networks, Renew. Energy, 33, 1622-1628, https://doi.org/10.1016/j.renene.2007.09.012, 2008.

Brest, C.L. and Goward, S.N.: Deriving surface albedo measurements from narrow band satellite data, Int. J. Remote Sens., 8, 351-367, https://doi.org/10.1080/01431168708948646, 1987.

Bristow, K.L. and Campbell, G.S.: On the relationship between incoming solar radiation and daily maximum and minimum temperature, Agric. For. Meteorol., 31, 159-166, https://doi.org/10.1016/0168-1923(84)90017-0, 1984.

Cañadas, E. M., Fenu, G., Peñas, J., Lorite, J., Mattana, E., and Bacchetta, G.: Hotspots within hotspots: 445 Endemic plant richness, environmental drivers, and implications for conservation, Biological Conservation, 170, 282-291, https://doi.org/10.1016/j.biocon.2013.12.007, 2014.

Chen, J.M., Liu, J., Cihlar, J., and Goulden, M.L.: Daily canopy photosynthesis model through temporal and spatial scaling for remote sensing applications, Ecol. Modell., 124, 99-119, https://doi.org/10.1016/S0304-3800(99)00156-8, 1999.

Chen, X., Su, Z., Ma, Y., Yang, K., and Wang, B.: Estimation of surface energy fluxes under complex terrain of Mt. Qomolangma over the Tibetan Plateau, Hydrol. Earth Syst. Sci., 17, 1607-1618, https://doi.org/10.5194/hess-17-1607-2013, 2013.

Diodato, N. and Bellocchi, G.: Modelling solar radiation over complex terrains using monthly climatological data, Agric. For. Meteorol. 144, 111-126, https://doi.org/10.1016/j.agrformet.2007.02.001, 2007.

https://doi.org/10.5194/essd-2020-250
Preprint. Discussion started: 28 October 2020

Donatelli, M., Bellocchi, G., and Fontana, F.: RadEst3.00: software to estimate daily radiation data from commonly available meteorological variables, European J. Agron., 18, 363-367, https://doi.org/10.1016/S1161-0301(02)00130-2, 2003.
Donatelli, M., Carlini, L., and Bellocchi. G.: A software component for estimating solar radiation, Environ. Modell. Software, 21(3), 411-416, https://doi.org/10.1016/j.envsoft.2005.04.002, 2006.
Dozier, J. and Frew, J.: Rapid calculation of terrain parameters for radiation modeling from digital elevation data, IEEE Trans. Geosci. Remote Sens., 28, 963-969, https://doi.org/10.1109/36.58986, 1990.
Dozier, J., Bruno, J., and Downey, P.: A faster solution to the horizon problem, Comp. Geosci., 7, 145-151, https://doi.org/10.1016/0098-3004(81)90026-1, 1981.
Dubayah, R.C.: Estimating net solar radiation using Landsat Thematic Mapper and digital elevation data, Water Resour. Res., 28, 2469-2484, https://doi.org/10.1029/92WR00772, 1992.
Dubayah, R.C.: Modeling a solar radiation topo climatology for the Rio Grande river watershed, J. Veg. Sci. 5, 627-640, https://doi.org/10.2307/3235879, 1994.
Dubayah, R.C. and van Katwijk, V.: The topographic distribution of annual incoming solar radiation in the Rio Grande river basin, Geophys. Res. Lett., 19(22), 2231-2234, https://doi.org/10.1029/92GL02284, 1992.
Dubayah, R. and Rich, P.M.: Topographic solar radiation models for GIS, Int. J. Geogr. Inf. Syst., 9, 405-413, https://doi.org/10.1080/02693799508902046, 1995.
El Ouderni, A.R., Maatallah, T., El Alimi, S., and Ben Nassrallah, S.: Experimental assessment of the solar energy potential in the gulf of Tunis, Tunisia, Renew. Sustain. Energy Rev., 20, 155-168, https://doi.org/10.1016/j.rser.2012.11.016, 2013.
Fu, P. and Rich, P.M.: A geometric solar radiation model and its applications in agriculture and forestry. In: Proceedings of the Second International Conference on Geospatial Information in Agriculture and Forestry, Lake Buena Vista, 10-12 January 2000, I-357-364, 2000.
Fu, P. and Rich, P.M.: A Geometric Solar Radiation Model with Applications in Agriculture and Forestry, Comput. Electr. Agric., 37, 25-35, https://doi.org/10.1016/S0168-1699(02)00115-1, 2002.
Geiger, M., Diabate, L., Menard, L., and Wald, L.: A web service for controlling the quality of measurements of global solar irradiation, Sol. Energy, 73, 474-480, https://doi.org/10.1016/S0038-092X(02)00121-4, 2002.
Goldberg, V. and Häntzschel, J.: Application of a radiation model for small-scale complex terrain in a GIS environment, Meteorol. Zeitschrift. 11(2), 119-128, https://doi: 10.1127/0941-2948/2002/0011-0119, 2002.
Hargreaves, G.H. and Samani, Z.A.: Estimating potential evapotranspiration, J. Irrig. Drain. Engin. 108 IR3, 223-230, 1982.
Herrero, J. and Polo, M. J.: Parameterization of atmospheric longwave emissivity in a mountainous site for all sky conditions, Hydrol. Earth Syst. Sci., 16, 3139–3147, https://doi.org/10.5194/hess-16-3139-2012, 2012.
Herrero, J. and Polo, M. J.: Evaposublimation from the snow in the Mediterranean mountains of Sierra Nevada (Spain), The Cryosphere, 10, 2981–2998, https://doi.org/10.5194/tc-10-2981-2016, 2016.
Herrero, J., Polo, M. J., Moñino, A., and Losada, M. A.: An energy balance snowmelt model in a Mediterranean site, J. Hydrol., 371, 98–107, https://doi.org/10.1016/j.jhydrol.2009.03.021, 2009.

Hewitt, G.M.: Mediterranean Peninsulas: the evolution of hotspots. In: Zachos, F.E. and Habel, J.C. (eds), Biodiversity hotspots: distribution and protection of conservation priority area, Springer, Berlin, pp. 123-147, 2011.

Heywood, V. H.: The Mediterranean flora in the context of world diversity, Ecología Mediterránea, 21, 11-18, 1995.

Ineichen, P. and Pérez, R.: A new airmass independent formulation for the Linke Turbidity coefficient, Sol. Energy, 73, 151-157, https://doi.org/10.1016/S0038-092X(02)00045-2, 2002.

Iqbal, M.: An introduction to solar radiation, Academic Press, Ontario, 1983.

Jacovides, C.P., Hadjioannou, L., Pashiardis, S., and Stefanou, L.: On the diffuse fraction of daily and monthly global radiation for the island of Cyprus, Sol. Energy, 56, 565-572, https://doi.org/10.1016/0038-092X(96)81162-5, 1996.

Journée, M. and Bertrand, C.: Quality control of solar radiation data within the RMIB solar measurements network, Sol. Energy, 85, 72-86, https://doi.org/10.1016/j.solener.2010.10.021, 2011.

Kasten, F. and Young, A.T.: Revised optical air mass tables and approximation formula, App. Optics, 28(22), 4735-4738, https://doi.org/10.1364/AO.28.004735, 1989.

Liu, M., Bárdossy, A., Li, J., and Jiang, Y.: GIS-based modelling of topography-induced solar radiation variability in complex terrain for data sparse region, Int. J. Geogr. Inf. Sci., 26(7), 1281-1308, https://doi.org/10.1080/13658816.2011.641969, 2012a.

Liu, J.D., Liu, J.M., Linderholm, H.W., Chen, D.L., Yu, Q., Wu, D.R., and Haginoya, S.: Observation and calculation of the solar radiation on the Tibetan Plateau, Energy Convers. Manag., 57, 23-32, https://doi.org/10.1016/j.enconman.2011.12.007, 2012b.

Liu, Y., Zhang, P., Nie, L., Xu, J., Lu, X., and Li, S.: Exploration of the Snow Ablation Process in the Semiarid Region in China by Combining Site-Based Measurements and the Utah Energy Balance Model-A Case Study of the Manas River Basin, Water, 11, 1058, https://doi.org/10.3390/w11051058, 2019

MacDonell, S., Kinnard, C., Mölg, T., Nicholson, L., and Abermann, J.: Meteorological drivers of ablation processes on a cold glacier in the semi-arid Andes of Chile, The Cryosphere, 7, 1513–1526, https://doi.org/10.5194/tc-7-1513-2013, 2013.

Mamassis, N., Efstratiadis, A., and Apostolidou, I.G.: Topography-adjusted solar radiation indices and their importance in hydrology, Hydr. Sc. J., 57(4), 756-775, https://doi.org/10.1080/02626667.2012.670703, 2012.

Martínez-Durbán, M., Zarzalejo, L.F., Bosch, J.L., Rosiek, S., Polo, J., and Batlles, F.J.: Estimation of global daily irradiation in complex topography zones using digital elevation models and meteosat images: Comparison of the results, Energy Convers. Manage. 50, 2233-2238, https://doi.org/10.1016/j.enconman.2009.05.009, 2009.

Moradi, I.: Quality control of global solar radiation using sunshine duration hours, Energy, 34, 1-6, https://doi.org/10.1016/j.energy.2008.09.006, 2009.

Mullen, R., Marshall, L., and McGlynn, B.: A Beta Regression Model for Improved Solar Radiation Predictions, J. Appl. Meteor. Climatol., 52, 1923-1938, https://doi.org/10.1175/JAMC-D-12-038.1, 2013.

Muneer, T., Younes, S., and Munawwar, S.: Discourses on solar radiation, Renew. Sust. Energy Rev., 11, 551-602, https://doi.org/10.1016/j.rser.2005.05.006, 2007.

https://doi.org/10.5194/essd-2020-250
Preprint. Discussion started: 28 October 2020

Myers, N., Mittermeier, R.A., Mittermeier, C.G., da Fonseca, G.A.B., and Kent, J.: Biodiversity hotspots for conservation priorities, Nature, 403, 853-858, https://doi.org/10.1038/35002501, 2000.

O'Farrell, P.J., Reyers, B., Le Maitre, D.C., et al.: Multi-functional landscapes in semi arid environments: implications for biodiversity and ecosystem services, Landscape Ecol., 25, 1231-1246, https://doi.org/10.1007/s10980-010-9495-9, 2010.

Oliphant, A.J., Spronken-Smith, R.A., Sturman, A.P., and Owens, I.F.: Spatial Variability of Surface Radiation Fluxes in Mountainous Terrain, J. App. Meteorol., 42, 113-128, https://doi.org/10.1175/1520-0450(2003)042<0113:SVOSRF>2.0.CO;2, 2003.

Pauli, H. et al.: Recent plant diversity changes on Europe's mountain summits, Science 336, 353-355, https://doi:10.1126/science.1219033, 2012.

Pérez-Palazón, M. J., Pimentel, R., Herrero, J., Aguilar, C., Perales, J. M., and Polo, M. J.: Extreme values of snow-related variables in Mediterranean regions: trends and long-term forecasting in Sierra Nevada (Spain), Proc. IAHS, 369, 157–162, https://doi.org/10.5194/piahs-369-157-2015, 2015.

Pérez-Palazón, M. J., Pimentel, R., and Polo, M. J.: Climate Trends Impact on the Snowfall Regime in Mediterranean Mountain Areas: Future Scenario Assessment in Sierra Nevada (Spain), Water, 10, 720, https://doi.org/10.3390/w10060720, 2018.

Pimentel, R., Herrero, J., and Polo, M.J.: Estimating snow albedo patterns in a Mediterranean site from Landsat TM and ETM+ images, In: Proceedings of the SPIE, Remote Sensing for Agriculture, Ecosystems, and Hydrology XV, 88870L, Dresden, Germany, 23-26 September 2013, doi:10.1117/12.2029064.

Pimentel, R., Herrero, J., and Polo, M.J.: Graphic user interface to preprocess Landsat TM, ETM+ and OLI images for hydrological applications. In: Proceedings of the HIC 2014, 11th International Conference on Hydroinformatics, New York, 17-21 August 2014.

Polo, M. J., Herrero, J., Pimentel, R., and Pérez-Palazón, M. J.: The Guadalfeo Monitoring Network (Sierra Nevada, Spain): 14 years of measurements to understand the complexity of snow dynamics in semiarid regions, Earth Syst. Sci. Data, 11, 393–407, https://doi.org/10.5194/essd-11-393-2019, 2019.

Ruiz-Arias, J.A., Tovar-Pescador, J., Pozo-Vázquez, D., and Alsamamra, H.: A comparative analysis of DEM-based models to estimate the solar radiation in mountainous terrain, Int. J. Geogr. Inf. Sci., 23, 1049-1076, https://doi.org/10.1080/13658810802022806, 2009.

Ruiz-Arias, J.A., Alsamamra, H., Tovar-Pescador, J., and Pozo-Vázquez, D.: Proposal of a regressive model for the hourly diffuse solar radiation under all sky conditions, Energy Convers. Manage., 51, 881-893, https://doi.org/10.1016/j.enconman.2009.11.024, 2010.

Ruiz-Arias, J.A., Pozo-Vázquez, D., Santos-Alamillos, F.J., Lara-Fanego, V., and Tovar-Pescador, J.A.: Topographic geostatistical approach for mapping monthly mean values of daily global solar radiation: A case study in southern Spain, Agric. For. Meteorol., 151, 1812-1822, https://doi.org/10.1016/j.agrformet.2011.07.021, 2011.

https://doi.org/10.5194/essd-2020-250
Preprint. Discussion started: 28 October 2020

Scaffetta, N. and Willson, R.C.: Multiscale comparative spectral analysis of satellite total solar irradiance measurements from 2003 to 2013 reveals a planetary modulation of solar activity and its nonlinear dependence on the 11 yr solar cycle, Pattern Recogn. Phys., 1, 123-133, doi: 10.5194/prp-1-123-2013, 2013.

Sheng, J., Wilson, J.P., and Lee, S.: Comparison of land surface temperature (LST) modeled with a spatially-distributed solar radiation model (SRAD) and remote sensing data, Environ. Modell. Software, 24(3), 436-443, https://doi.org/10.1016/j.envsoft.2008.09.003, 2009.

Šùri, M. and Hofierka, J.: A new GIS-based solar radiation model and its application to photovoltaic assessments, Trans. GIS, 8(2), 175-190, https://doi.org/10.1111/j.1467-9671.2004.00174.x, 2004.

Tang, W., Yang, K., Qin, J., Li, X., and Niu, X.: A 16-year dataset (2000–2015) of high-resolution (3 h, 10 km) global surface solar radiation, Earth Syst. Sci. Data, 11, 1905–1915, https://doi.org/10.5194/essd-11-1905-2019, 2019.

Tomas-Burguera, M., Vicente-Serrano, S. M., Beguería, S., Reig, F., and Latorre, B.: Reference crop evapotranspiration database in Spain (1961–2014), Earth Syst. Sci. Data, 11, 1917–1930, https://doi.org/10.5194/essd-11-1917-2019, 2019.

Tovar. J., Olmo, F.J., and Alados-Arboledas, L.: Local scale variability of solar radiation in a mountainous region, J. App. Meteorol., 34, 2316-2322, https://doi.org/10.1175/1520-0450(1995)034<2316:LSVOSR>2.0.CO;2, 1995.

Tovar-Pescador, J., Pozo-Vázquez, D., Ruiz-Arias, J.A., Batllés, J., López, G., and Bosch, J.L.: On the use of the digital elevation model to estimate the solar radiation in areas of complex terrain, Meteorol. Appl., 13, 279-287, https://doi.org/10.1017/S1350482706002258, 2006.

Wilson, J.P. and Gallant, J.C.: Secondary topographic attributes. In: Wilson, J.P. and Gallant, J.C. (eds), Terrain Analysis: Principles and Applications, John Wiley & Sons, New York, pp. 51-85, 2000.

Winslow, J.C., Hunt, E.R., and Piper, S.C.: A globally applicable model of daily solar irradiance estimated from air temperature and precipitation data, Ecol. Modell., 143, 227-243, https://doi.org/10.1016/S0304-3800(01)00341-6, 2001.

Wu, G.F., Liu, Y.L., and Wang, T.J.: Methods and strategy for modeling daily global solar radiation with measured meteorological data-A case study in Nanchang station, China, Energy Convers. Manage., 48, 2447-2452, https://doi.org/10.1016/j.enconman.2007.04.011, 2007.

Yang, K. and Koike, T.: A general model to estimate hourly and daily solar radiation for hydrological studies., Water Resour. Res. 41(10), W10403, doi: 10.1029/2005WR003976, https://doi.org/10.1029/2005WR003976, 2005.

Yang, K., Koike, T., and Ye, B.: Improving estimation of hourly, daily, and monthly solar radiation by importing global data sets, Agric. For. Meteorol., 137, 43-55, https://doi.org/10.1016/j.agrformet.2006.02.001, 2006.

Yang. K., He, J., Tang, W.J., and Qin, J. and Cheng, C.C.K.: On downward shortwave and longwave radiations over high altitude regions: Observation and modeling in the Tibetan Plateau, Agric. For. Meteorol., 150, 38-46, https://doi.org/10.1016/j.agrformet.2009.08.004, 2010.

Younes, S., Claywell, R., and Muneer, T.: Quality control of solar radiation data: present status and proposed new approaches, Energy, 30, 1533-1549, https://doi.org/10.1016/j.energy.2004.04.031, 2005.

https://doi.org/10.5194/essd-2020-250
Preprint. Discussion started: 28 October 2020

Appendix A. Solar radiation equations

The sequence followed by the model is summarized in Figure A1. Computations are classified at the point scale of weather stations (Point) and the distributed scale of grids of the Digital Elevation Model (DEM) (Distributed). The complete explanation of the algorithms and assumptions of the model can be found in detail in Aguilar et al. (2010).

Firstly, daily extraterrestrial radiation (R_{ext} in MJ m^{-2} day^{-1}) is computed by integrating the extraterrestrial radiation incident upon a horizontal surface relative to the sun's beams from sunrise to sunset (Eq. A1).

$$R_{ext} = E_o \cdot I_{SC} \cdot \cos(\theta_z) \quad \text{(A1)}$$

where I_{SC} is the solar constant (1367 W m^{-2}), θ_z is the zenith angle and E_o, the eccentricity factor. These variables were computed following the equations in Dozier et al. (1981).

Then, the daily clearness index (CI), as the ratio of observed daily global radiation (R_{go} in MJ m^{-2} day^{-1}) to the daily extraterrestrial radiation, is computed at each weather station (Eq. A2).

$$CI = R_{go} / R_{ext} \quad \text{(A2)}$$

CI is expressed in terms of two factors, CI_{CS} and fCI_{cl}. The first term represents the influence of atmosphere under clear-sky conditions over solar radiation, while the second term includes the cloudiness effects that decrease the final incoming solar radiation (Eq. A3). The approximation of Ineichen and Perez (2002) is used to compute the global radiation under clear-sky conditions, R_{gcs}, and thus, distributed hourly R_{gcs} values are obtained from the sun elevation angle, the height of the cell, the Linke turbidity factor (T_L) and the atmospheric mass obtained following the parameterization of Kasten and Young (1989). Thus, hourly CI_{CS} values can be computed cell by cell and then the mean daily distributed values are generated. Once daily CI and CI_{CS} values are known, fCI_{cl} is obtained at each weather station from Eq. A3 and spatially distributed following the inverse distance weighted (IDW) method. From daily CI_{CS} and fCI_{cl} maps, daily distributed CI and R_g values can be obtained at cell scale from Eq. A3 and A4.

$$CI = CI_{CS} \cdot fCI_{cl} \quad \text{(A3)}$$

$$R_g = R_{ext} \cdot CI_{CS} \cdot fCI_{cl} \quad \text{(A4)}$$

Topographic effects need to be evaluated for the different sun positions during the day and thus, hourly values of the different components need to be derived. Two different procedures are currently available in the model. The first one proposed in Aguilar et al. (2010) applies Jacovides et al. (1996) (Eq. A5.1) to produce the daily diffuse (R_d in MJ m^{-2} day^{-1}) and daily beam

https://doi.org/10.5194/essd-2020-250
Preprint. Discussion started: 28 October 2020

Open Access Earth System Science Data Discussions

values (R_b in MJ m^{-2} day^{-1}). The model finally computes hourly beam and diffuse values on horizontal surfaces (r_b and r_d, both in MJ m^{-2} h^{-1}), from the daily amounts and following the temporal pattern of extraterrestrial hourly radiation during the day.

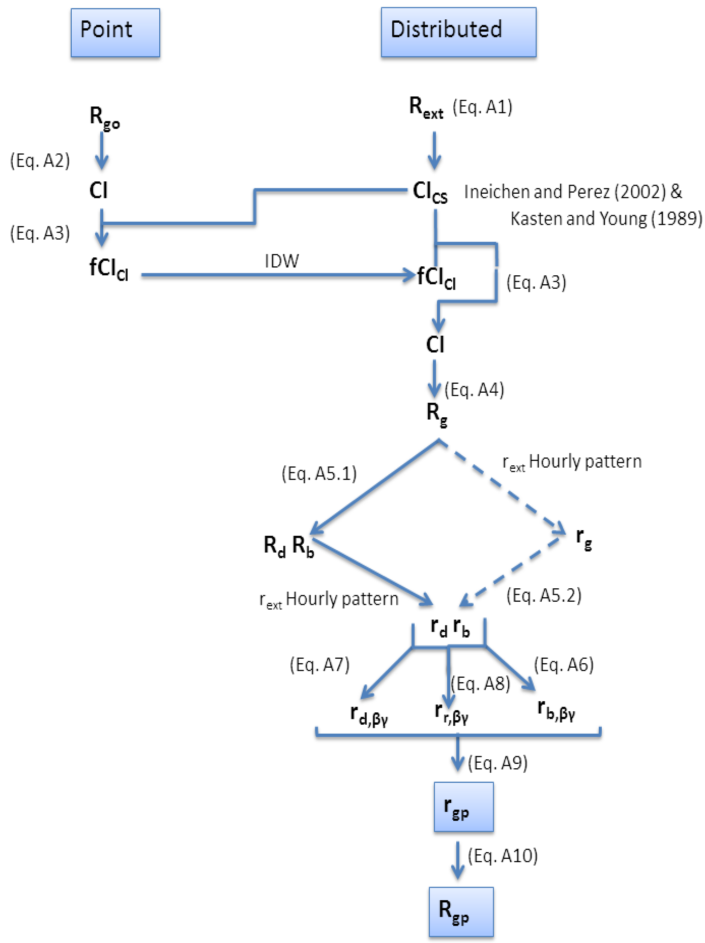

Figure A1. Flow chart of the solar radiation model

$$\frac{R_d}{R_g} = \begin{cases} 0.992 - 0.0486CI & CI \le 0.1 \\ 0.954 + 0.734CI - 3.806CI^2 + 1.703CI^3 & 0.1 < CI \le 0.71 \\ 0.165 & CI > 0.71 \end{cases} \qquad \text{(A5.1)}$$

The second approach uses the temporal pattern of extraterrestrial hourly radiation, r_{ext}, to generate hourly global values, r_g according to previous studies (Chen et al., 1999; Ruiz-Arias et al., 2011). Then, the hourly regressive model developed by Ruiz-Arias et al. (2010) is applied to estimate the hourly diffuse values (Eq. A5.2) from the hourly CI, CI_h, as the ratio of r_g to

https://doi.org/10.5194/essd-2020-250
Preprint. Discussion started: 28 October 2020

r_{ext}. This model was implemented as it has been validated over Europe and USA using ground data from different sites, including some Spanish stations (Ruiz-Arias et al., 2010). Hourly beam values (r_b) are thus obtained on a cell basis as the difference between global and diffuse hourly radiation distributed values.

$$\frac{r_d}{r_g} = 0.952 - 1.041 e^{-\exp(2.3 - 4.702 \cdot CI_h)} \quad \text{(A5.2)}$$

First applications at the study site have shown negligible differences between both partitioning schemes. The differences with daily recorded data were insignificant in the second decimal place of error values. Thus, the results presented in this study were obtained with the original scheme of Aguilar et al. (2010) (Eq. A5.1) while the authors continue working on the improvement on the partitioning scheme of the model.

Then, the topographic correction is carried out and depending on the component, different procedures are applied.

Hourly beam radiation on a surface of slope β and orientation γ, ($r_{b,\beta\gamma}$ in MJ m^{-2} h^{-1}), is calculated according to Eq. A6. in terms of r_b, θ_z and a new corrected zenith angle for the sloping surface, θ (Iqbal, 1983). Then, the model checks the shading effects. Self-shading will occur if the angle between the normal to the surface and the solar vector is greater than 90 degrees. Finally, shading by nearby terrain takes place when the illumination angle is greater than the horizon angle in the same direction. The model previously obtains the horizons following the algorithms of Dozier et al. (1981) and Dozier and Frew (1990), by comparing the slopes between cells in the eight directions.

$$r_{b,\beta\gamma} = r_b \left(\cos\theta / \cos\theta_z \right) \quad \text{(A6)}$$

Hourly diffuse radiation on a surface of slope β and orientation γ ($r_{d,\beta\gamma}$ in MJ m^{-2} h^{-1}), is calculated according to Eq. A7 in terms of r_d and SVF, the sky view factor, that modifies the incoming radiation incident on a flat surface to consider possibly obstruction effects on a sloping surface (Dubayah, 1992). Dozier and Frew (1990) obtained an analytical expression for the estimation of the SVF in terms of the different horizons in each direction considered assuming an isotropic sky.

$$r_{d,\beta\gamma} = r_d \cdot SVF \quad \text{(A7)}$$

Finally, hourly reflected radiation on a surface of slope β and orientation γ ($r_{r,\beta\gamma}$ in MJ m^{-2} h^{-1}) and albedo ρ is calculated according to Dozier and Frew (1990) as expressed in Eq. A8.

$$r_{r,\beta\gamma} = \rho \cdot \left[\frac{1+\cos\beta}{2} - SVF \right] \cdot (r_d + r_b) \quad \text{(A8)}$$

Hourly global distributed radiation (r_{gp} in MJ m^{-2} h^{-1}) is obtained by addition of the three hourly components at each cell according to Eq. A9.

https://doi.org/10.5194/essd-2020-250
Preprint. Discussion started: 28 October 2020

$$r_{gp} = r_{b,\beta\gamma} + r_{d,\beta\gamma} + r_{r,\beta\gamma} \quad \text{(A9)}$$

Finally, daily global distributed radiation (R_{gp} in MJ m^{-2} day^{-1}) is obtained as the summation of hourly global distributed radiation values (Eq. A10).

$$R_{gp} = \sum_{24h} r_{gp} \quad \text{(A10)}$$

Appendix B: Nomenclature

Symbols

CI: daily clearness index

CI_{CS}: daily clearness index in a cloudless atmosphere

CI_h: hourly clearness index

E_o: eccentricity factor

fCI_{cl}: cloudiness effects factor

I_{SC}: solar constant

k: diffuse to global irradiance ratio

N CI<0.3: rate of days for cloudy conditions

N 0.3<CI<0.6: rate of days for partially cloudy conditions

N CI>0.6: rate of days for clear-sky conditions

N_o: number of initially available daily records in the study period

N: number of available daily records after the quality check

Q_1: Quartile 1

Q_3: Quartile 3

R_b: daily beam radiation

R_d: daily diffuse radiation

R_{ext}: daily extraterrestrial radiation

R_g: global radiation

R_{gcs}: global radiation under clear-sky conditions

R_{go_max}: maximum daily global radiation observed value

R_{go_mean}: mean daily global radiation observed value

R_{go_min}: minimum daily global radiation observed value

R_{gp}: daily global radiation predicted by the model

r_b: hourly beam radiation on horizontal surfaces

https://doi.org/10.5194/essd-2020-250
Preprint. Discussion started: 28 October 2020

$r_{b,\beta\gamma}$: hourly beam radiation on a surface of slope β and orientation γ

r_d: hourly diffuse radiation on horizontal surfaces

$r_{d,\beta\gamma}$: hourly diffuse radiation on a surface of slope β and orientation γ

r_{ext}: hourly extraterrestrial radiation

$r_{r,\beta\gamma}$: hourly reflected radiation on a surface of slope β and orientation γ

r_g: hourly global radiation on horizontal surfaces

r_{gp}: hourly global radiation predicted by the model

R^2: coefficient of determination

T_L: Linke turbidity factor

z: elevation

Abbreviations

DEM: Digital Elevation Model

IDW: Inverse Distance Weighted

RMSE: Root Mean Square Error

SN: Sierra Nevada mountain range

SVF: Sky view factor

UPH: Unsolved Problems in Hydrology

Greek symbols

α: slope of the fit between R_{gp} and R_{go}

β: slope

γ: orientation

ρ: albedo

θ: corrected zenith angle for the sloping surface

θ_z: zenith angle